IJHSR
ijhighschoolresearch.org
RESEARCH ARTICLE

Automated Biomedical Waste Segregation with Residual Neural Networks

Srivatsav Kannan

The Indian Public School, 193 Sathy Road, Kovilpalayam, Tamil Nadu, 641107, India; srivatsavkannan@gmail.com

ABSTRACT: The rapid growth in Biomedical Waste (BMW) generation poses significant challenges to effective BMW management, impacting the health and safety of healthcare and sanitation workers, patients, and the public. Segregating BMW at the source is critical to the BMW management system. However, in developing countries like India, less than half of the BMW is segregated at the source due to logistical challenges associated with manual segregation. This study addresses these challenges by developing a deep learning model for automated BMW segregation based on the Indian Government's Biomedical Waste Management Rules, 2016. To achieve this, the BMW-Seg-India dataset was created with images collected from a multi-specialty hospital in India and other publicly available datasets and organized into four classes: yellow, red, white, and blue, in line with the guidelines. A novel deep-learning model, BMWNet52, employing a modified ResNet50 architecture, was trained with transfer learning on the dataset. The model achieved an accuracy of 97.99% in classifying the four categories, demonstrating that this deep-learning classifier is an effective solution for automated BMW segregation. The findings could lead to a fully autonomous BMW management system, integrating automated segregation and disposal, minimizing exposure to hazardous waste, and enhancing efficiency worldwide.

KEYWORDS: Robotics and Intelligent Machines; Machine Learning; Biomedical Waste Management; Automated Waste Segregation; BMW Management Rules India.

Introduction

The World Health Organization (WHO) 2023 Global Progress Report on Water, Sanitation, and Hygiene (WASH) in healthcare facilities indicates that only 34% of countries have hospital facilities capable of segregating and treating Biomedical Waste (BMW).[1] The magnitude of the BMW generation is huge, with nearly 16 billion injections administered yearly,[2] representing just one category of BMW. In high-income countries, the rate of BMW generation is nearly 11 kg/bed/day, whereas in low-income countries, it is 6 kg/bed/day. However, the amount of hazardous waste is significantly higher because of improper handling.[3] In India, 619 tons of BMW were generated daily in 2019. The increasing number of healthcare facilities (HCFs) and the prevalence of single-use equipment further drive this growth in waste generation.[4,5]

The irresponsible management of BMW leads to the spread of infections, posing a significant risk to the health and safety of healthcare workers, individuals handling such waste, and patients.[6] However, these infections are not limited to a healthcare setting, with diseases potentially spreading among the general population, leading to far-reaching public health consequences.[7] Every year, approximately 5.2 million people, including about 4 million children, die from exposure to Biomedical Waste.[8] The World Health Organization's (WHO) core principles for achieving safe and sustainable management of healthcare waste estimated that 32% of new Hepatitis B infections, 40% of Hepatitis C infections, and 5% of new Human Immunodeficiency Virus (HIV) infections were caused by contaminated syringes, amounting to 23 million infections worldwide.[9]

Only 10-25% of the BMW generated is hazardous, and nearly 75-90% is non-hazardous or general waste. However, if the BMW is not appropriately segregated at the source, all of the waste generated becomes hazardous, thus significantly increasing the volume of biohazardous waste.[6] This increases the burden on sanitation workers and endangers their health, hindering proper disposal.[10] This underscores the importance of segregation in the BMW management system.

In July 1998, the Government of India announced its first BMW management rules, amended in 2000, 2003, and 2011. This was superseded by the Bio-Medical Waste Management Rules, 2016, with subsequent amendments in 2018 and 2019, which simplified the categorization of BMW and outlined segregation and disposal methods.[6,11,12] Despite the new regulations, less than 50% of BMW is segregated at its source in India. Furthermore, the share of workers who received training in BMW management is under 20%, one of the lowest in the world. These logistical challenges are caused by manual segregation's inherent limits and lack of technological adaptation.[13]

Automated BMW segregation using AI can address these challenges. This involves image classification, for which deep-learning models are widely used.[14] Deep learning architectures for image classification have developed significantly over the years. Early CNNs, such as LeNet-5, AlexNet, and VGGNet, laid the foundation for subsequent advancements. To address issues with these models, such as the vanishing gradient problem, ResNets and DenseNets were developed.[15] Deep learning-based image classifiers have also been developed for BMW classification with good results.[16] One approach utilizes the ResNeXt architecture, a variant of the more widely

  DOI: 10.36838/v6i10.11

known ResNet architecture, along with a BMW dataset from China to achieve an accuracy of 97.12% in classifying 8 kinds of BMW.[17]

However, a comprehensive dataset and a deep learning approach are still needed to classify BMW according to the Indian Government's Biomedical Waste Management Rules, 2016, and subsequent amendments. This study aims to develop the first deep learning model that can classify BMW images into four categories: yellow, red, white, and blue, as outlined by the Indian Government's guidelines,[12] by training on a comprehensive BMW dataset created based on these guidelines.

Methods

Data collection:

For this research, a custom dataset, named BMW-Seg-India, was compiled and manually annotated to encompass a comprehensive representation of biomedical waste as per Schedule I of The Biomedical Waste Management Rules, 2016.[12] The rules stipulate that BMW should be segregated into 4 color-coded bins, as displayed in Table 1.[6]

Table 1: An outline of Schedule I of BMW Management Rules 2016.[12] It displays all the categories and types of BMW considered in this study.

Category	Type of Waste	Examples
Yellow	Human anatomical waste, Soiled waste, Expired or discarded medicines, Chemical waste, Discarded linens, and Microbiological/lab waste	Human tissue, discarded tablets and capsules, tissue cultures, blood bags, contaminated bed sheets
Red	Contaminated, recyclable waste	Plastic tubing, urine bags, vacutainers, syringes with needles cut, gloves, catheters
White	Waste sharps (including metals)	Syringes with fixed needles, scalpels, blades, needles
Blue	Glassware, Metallic implants	Used glass bottles, plates and screws

All types of waste from Schedule I of BMW management 2016 rules[12] were included in this study except for Animal anatomical waste and Chemical liquid waste in the yellow category. Animal anatomical waste was not considered; only biomedical waste from human medical centers was collected. Chemical liquid waste was not considered because it is not disposed of in the bin. Furthermore, while annotating the dataset, a distinction could not be made between cytotoxic waste, which requires a yellow bin with a cytotoxic sticker, and regular waste in the yellow category, as there are no visually distinguishable features between the two.

The BMW-Seg-India dataset was organized into 4 classes, representing the 4 BMW categories in Table 1, with images from each considered waste type adequately represented. Images for the dataset were collected from Kovai Medical Center and Hospital (KMCH), a multi-specialty hospital in Coimbatore, India, in 2024. Images were also sourced from publicly available internet datasets: Medical Waste 4.0,[18] Pharmaceutical and Biomedical Waste,[19] TrashBox,[20] and waste_pictures.[21]

Each dataset from the internet contained images of various categories. These were manually annotated and added to the BMW-Seg-India dataset, as shown in Table 2.

Table 2: Annotation of the biomedical waste images sourced from the Internet datasets. It displays the category—Yellow, Red, White, or Blue—assigned to each image type in the Internet dataset, per the BMW Management Rules, 2016.[12]

Dataset	Yellow	Red	White	Blue
Medical Waste 4.0[18]	Gauzes, medical caps, medical glasses, medical shoe covers	Gloves, medical filters, urine bags	Not available	Test tubes
Pharmaceutical and Biomedical Waste[19]	Body tissue or organ, gauze, mask	Gloves, syringe	Metal equipment, syringe needles, tweezers	Glass equipment
TrashBox[20]	Masks, medicine	Gloves	Syringe - fixed needle	Not available
waste_pictures[21]	Band-Aid, tablet capsule, plastic medicine bottles	Not available	Not available	Glass medicine Bottles

All 6324 images from the Medical Waste 4.0 dataset were used.[18] The Pharmaceutical and Biomedical Waste dataset consisted of 12 classes.[19] Out of the 12 classes, 3 classes - organic waste, plastic equipment packaging, and paper equipment packaging - were discarded because they contained general waste as per the BMW 2016 guidelines and did not meet the criteria to be included in any of the 4 classes in the BMW-Seg-India dataset. From the other 9 classes, 3935 images were reorganized and used in the dataset.

Images of discarded medicines, a type of waste in the yellow category, could not be acquired from the above-mentioned medical waste datasets. Therefore, 2 general waste datasets were also used. The TrashBox dataset consisted of 7 classes of waste,[20] of which 6 classes represented general waste and were discarded, and 1565 images from the medical waste class were used in the BMW-Seg-India dataset.

Another dataset, named waste_pictures,[21] contained 34 classes, of which 3 classes were used for this study, adding 2041 images. In the medicine bottle class, glass medicine bottles were manually identified and used for the blue class, whereas other medicine bottles were used for the yellow class.

Prior to any augmentation or curation, the Internet dataset consisted of 14,267 images. The distribution across the classes was as follows: Yellow—6247, Red—5601, White—1504, Blue—915. The samples from the Internet dataset are shown in Figure 1.

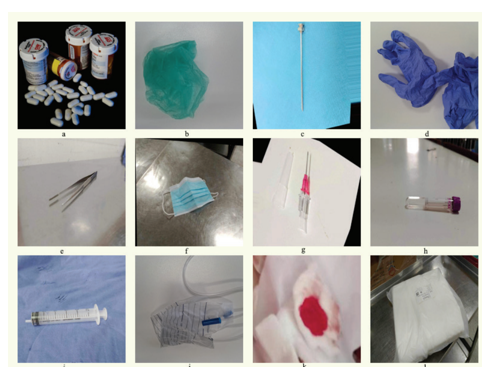

Figure 1: Biomedical waste image samples sourced from the internet datasets, including bin categories. (a) Discarded medicines (Yellow), (b) Cap (Yellow), (c) Needle (White), (d) Gloves (Red), (e) Metal sharp (White), (f) Mask (Yellow), (g) Fixed needle syringe (White), (h) Medicine vial (Blue), (i) Syringe with needle cut (Red), (j) Urine bag (Red), (k) Dressing (Yellow), (l) Discarded linen (Yellow).

Certain waste types in Table 1 could not be sourced from the internet datasets. In the yellow category, images of chemical and microbiological waste were absent; in the red category, images of vacutainers, IV equipment, and catheters were absent. There were also no images of metallic implants, a type of waste in the blue category.

To ensure that BMW was equally represented across all considered categories and to incorporate data specific to India, additional medical waste images were collected from KMCH, a multi-specialty hospital in Coimbatore, India. Images of biomedical waste were photographed, with an iPhone 12 camera, from various labs and wards within the hospital. Images containing multiple waste types were processed using the Preview app. The images were cropped into individual waste instances for accurate categorization.

These images were manually annotated and integrated into the BMW-Seg-India dataset as described in Table 3.

Table 3: Annotation of the biomedical waste images photographed at the local hospital. It displays the category—Yellow, Red, White, or Blue—assigned to each image type collected from the local hospital, per the BMW Management Rules, 2016.[12]

Hospital site	Yellow	Red	White	Blue
Phlebotomy Lab	Cotton swabs	Syringes with needles cut, gloves, vacutainers	Syringe Needles	Not available
Histopathology Lab	Chemical waste, discarded linens, masks	Gloves	Not available	Glass slides, glass bottles
Biochemistry Lab	Chemical waste	Syringes, gloves	Not available	Test tubes, medicine vial, glass bottles
Microbiology Lab	Chemical waste, laboratory cultures	Gloves	Not available	Glass bottles
Wards	Human anatomical waste, blood bags, discarded medicines, discarded linens cotton swabs,	IV equipment, catheters, urine bags, gloves, syringes with needles cut	Needles, Metal sharps	Medicine vials, glass ampoules
Orthopedic department	Plaster casts	Not available	Not available	Metallic implants, plates and screws

After collection, annotation, and processing, the dataset from the local hospital consisted of 701 images, with 175 in the yellow class, 197 in the red class, 72 in the white class, and 257 in the blue class. The image samples from the local hospital dataset are shown in Figure 2.

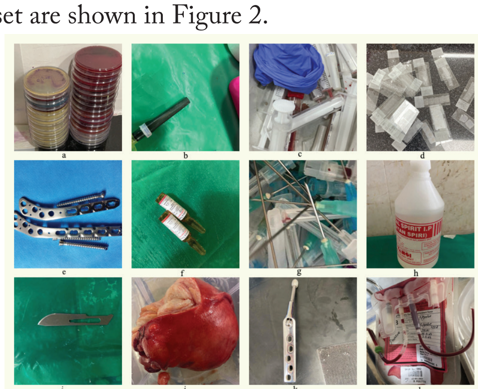

Figure 2: Biomedical waste image samples collected from the local hospital including bin categories. (a) Laboratory cultures (Yellow), (b) Vacutainer (Red), (c) Syringes and Glove (Red), (d) Glass slides (Blue), (e) Metallic implants (Blue), (f) Ampoules (Blue), (g) Needles (White), (h) Chemical waste (Yellow), (i) Blade (white), (j) Anatomical waste (Yellow), (k) Metallic implant (Blue), (l) Blood bag (Yellow).

Data Augmentation:

Before augmentation, the internet dataset was manually curated to ensure high quality. First, images containing multiple waste samples were manually segmented into individual images. Then, low-quality images that were not representative of biomedical waste in a real hospital setting were discarded.

After curation, the internet dataset contained 4925 images for the red class, significantly higher than samples for the white and blue classes at 1461 images and 938 images, respectively. The number of images in the yellow class was close to that in the red class, at 3708. A data augmentation framework was implemented to address these significant class imbalances in the blue and white classes, as the imbalances could have affected the model's performance in the underrepresented classes.[22] Transformations such as rotation, translation, rescaling, brightness adjustments, and flipping were applied to existing images from underrepresented classes, by using the ImageDataGenerator class from the Keras preprocessing library, to generate new images. These transformations ensured the new images possessed varied features so the model could generalize effectively. As a result, this augmentation process mitigated the class imbalance gap, leading to a more balanced dataset comprising 4383 images for the White class and 3752 images for the Blue class.

Images collected from the hospital were augmented because larger datasets typically lead to better results during training.[23] After augmentation, the resulting dataset consisted of 875 images in the yellow class, 985 in the red class, 360 in the white class, and 1285 in the blue class.

The final BMW-Seg-India dataset used for training consisted of 20273 images across all 4 classes, with 4583 images in the yellow class, 5910 images in the red class, 4743 images in the white class, and 5037 images in the blue class. The overall workflow for creating the dataset is shown in Figure 3.

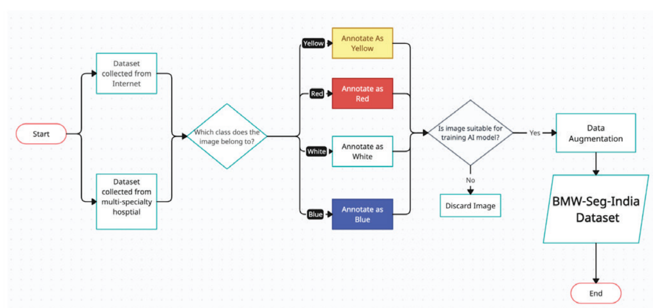

Figure 3: Dataset creation workflow. Diagram shows the workflow of collecting, annotating, curating, and augmenting images before adding them to the BMW-Seg-India dataset.

Model Architecture and Training:

A residual network (ResNet) architecture was chosen for the BMW image classification task because it generally offers high accuracy for image classification and mitigates overfitting.[17, 24-26] The ResNet architecture facilitated the use of a deeper model for the segregation task by mitigating the vanishing gradient problem, an issue faced by traditional deeper neural networks, where the gradients used to update the network weights become too small.[15, 27]

DOI: 10.36838/v6i10.11

For the image classification task, the ResNet architecture was used to capture the image features through blocks consisting of multiple convolutional layers. Skip connections that provide shortcuts between layers facilitated a proper training process without vanishing gradients. The goal was for the model to learn residual mappings in addition to linear mappings. Mathematically, this can be expressed as:

$$y = F(x, \{W_i .... W_n\}) + x$$

Here, x and y denote the input and output of the block, respectively, F represents the mapping to be learned, and the vector {W} denotes the weights of the block's layers, which are also updated through training. This residual block is visualized in Figure 4.

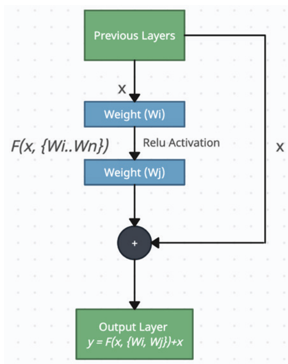

Figure 4: Representation of the residual block structure in the model. This is the repeating unit of the residual network architecture.

ResNet50 is a variation of the ResNet architecture with 50 layers.[28] The ResNet50 has generally outperformed the other residual networks due to increased depth and other modifications in architecture. This has made ResNet50 one of the best image classification models and a good choice for this image classification task.[29]

Transfer learning was used to train the ResNet50 model because it provides better performance and generalization for image classification tasks than training from scratch.[30,25] Transfer learning provides much faster training and convergence despite limited computational resources, as it involves fine-tuning a pre-trained model for the BMW segregation task.[31] This study chose a ResNet50 model pre-trained on the ImageNet dataset.[32]

Before training, a Global Average Pooling layer was added to the model. This layer was employed to effectively downsample the spatial dimensions of the feature maps generated by the pre-trained 50 layers to simplify the data while retaining essential information about the BMW image samples. The Global Average Pooling layer was used to output the spatial averages of all the previous convolutional layers. By acting as a structural regularizer, it automatically mitigated overfitting.[33] For this reason, it was chosen over a traditional fully connected layer, which would have required additional dropout layers to prevent overfitting. These dropout layers would have increased the time required for convergence and decreased the accuracy of the model.[34]

A final dense layer was added to fine-tune the model and produce the classification output. This dense layer was set to have 4 units, corresponding to the 4 BMW classes in the BMW-Seg-India dataset, and was chosen to have a softmax activation function. The softmax function was used to ensure that the model output is a probability distribution across these 4 classes,[35] enabling the model to predict the likelihood of a given image belonging to a specific class. The dense layer was the only trainable layer, as the 50 pre-trained layers were frozen to reduce the training time.

To prevent overfitting while training the model, the Adam optimizer was employed,[36] which allowed the automatic updation of the learning rate based on the magnitude of the gradients leading up to that epoch. The Adam optimizer has been found to provide the best performance, particularly for image classification in a healthcare context,[37] making it a good choice for this task. Mathematically, the Adam optimizer updates the model parameters by using the following rule:

$$\theta_{t+1} = \theta_t - (\eta/(\sqrt{vt} + \epsilon))mt$$

Where θ_t represents the model parameters at iteration t, η denotes the learning rate, mt denotes the first-order moment estimate (mean of all previous gradients), vt denotes the second-order moment estimate (variance of all previous gradients), and ϵ is a small constant to prevent division by zero.[36]

Sparse categorical cross-entropy was used as the loss function to train the model because it performs well for multi-class classification tasks.[38] During training, the loss was calculated by computing the cross-entropy between the true labels and the predicted probabilities for each class. The following equation can represent this:

$$L(y, \widehat{y}) = -1/N * \sum_{i=1}^{N} \sum_{j=1}^{C} y_{ij} * log(\widehat{y}_{ij})$$

In this equation, N represents the number of BMW image samples, C is equal to the number of classes in the dataset (4 BMW classes), y_{ij} is the ground truth equal to 1 if sample i belongs to class j and 0 otherwise, and $\hat{y}_{ij}$ is the predicted probability of sample i belonging to class j as produced by the model.[39]

The augmented BMW images were resized to 224x224 after experimenting with different image resolutions: 512x512, 256x256, and 128x128. The image size of 224x224 exhibited the best performance. 70% of the data was allocated for the training set and the remaining 30% for the validation set, ensuring sufficient images for training and testing. This split was performed after randomly shuffling the dataset to prevent any bias.

The model was then trained for 20 epochs with the Apple M3 GPU, with early stopping implemented as a model callback to determine the epoch at which the validation accuracy reached its peak. This prevented overfitting and found the best version of the model. The trained model was named BMWNet52, reflecting the total number of layers in the architecture. The overall BMWNet52 model training workflow and architecture are shown in Figure 5.

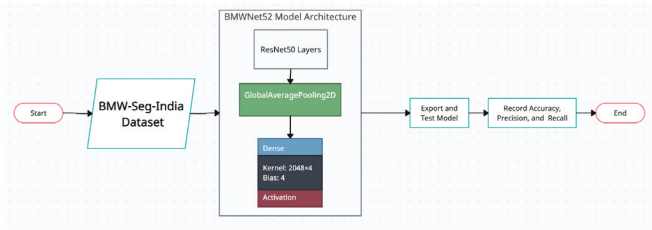

Figure 5: The process of training and testing the BMWNet52 model. Images from the BMW-Seg-India Dataset were used for training the BMWNet52 model. The model was then exported and tested to generate the final performance metrics.

Result and Discussion

The BMWNet52 model achieved an overall validation accuracy of 97.99%.

Table 4 showcases the model's efficacy for this BMW classification task by displaying a range of metrics representing the overall performance and the performance of specific classes.

Table 4: The metrics of the BMWNet52 model on the validation set of the BMW-Seg-India dataset. The model performed well across all classes, with a high Precision, Recall, and F1-Score.

Class	Precision	Recall	F1-Score	Support (Images)
Yellow	96.65%	97.15%	96.90%	1367
Red	97.9%	98.06%	97.98%	1755
White	98.59%	98.59%	98.59%	1420
Blue	98.76%	98.12%	98.44%	1539
Macro Avg	97.97%	97.89%	97.98%	6081
Weighted Avg	98.00%	97.99%	97.99%	6081

Analysis Metrics:

The support metric represents the number of images in each class, with the entire validation set used for averaging.

Accuracy measures the proportion of correctly classified instances among the total instances across all classes. In this case, it is defined by the formula:

$$Accuracy = ((TP_Y + TP_R + TP_W + TP_B) / N) * 100$$

TP_Y, TP_R, TP_W, and TP_B represent the number of instances correctly predicted as yellow, red, white, and blue, respectively. The variable N represents the total number of images.

The precision for each class measures the proportion of correctly predicted instances of that class out of all the instances predicted as that class. It is calculated as the ratio of True Positives to the sum of True Positives and False Positives for each class.

$$Precision_Y = TP_Y / (TP_Y + FP_Y) * 100$$

$$Precision_R = TP_R / (TP_R + FP_R) * 100$$

$$Precision_W = TP_W / (TP_W + FP_W) * 100$$

$$Precision_B = TP_B / (TP_B + FP_B) * 100$$

The Recall for each class measures the proportion of correctly predicted instances of that class out of all the actual instances. It is calculated as the ratio of True Positives to the sum of True Positives and False Negatives for each class.

$$Recall_Y = TP_Y / (TP_Y + FN_Y) * 100$$

$$Recall_R = TP_R / (TP_R + FN_R) * 100$$

$$Recall_W = TP_W / (TP_W + FN_W) * 100$$

$$Recall_B = TP_B / (TP_B + FN_B) * 100$$

The F1 Score for each class is the harmonic mean of the Precision and Recall for that class. It provides a balance between Precision and Recall.

$$F1Score_Y = 2 * (Precision_Y * Recall_Y) / (Precision_Y + Recall_Y)$$

$$F1Score_R = 2 * (Precision_R * Recall_R) / (Precision_R + Recall_R)$$

$$F1Score_W = 2 * (Precision_W * Recall_W) / (Precision_W + Recall_W)$$

$$F1Score_B = 2 * (Precision_B * Recall_B) / (Precision_B + Recall_B)$$

Macro and weighted averages were calculated to represent these metrics across all dataset classes.

For macro-averaging, the average of the metrics across all classes was calculated. This gives equal weight to each class regardless of the number of images in that class.

$$Macro\ Averaged\ Precision = (1 / N) * \Sigma\, Precision_i$$

$$Macro\ Averaged\ Recall = (1 / N) * \Sigma\, Recall_i$$

$$Macro\ Averaged\ F1\ Score = (1 / N) * \Sigma\, F1\ Score_i$$

Weighted averaging considers the number of images in each class by taking a weighted average of the metrics based on the support for each class.

$$Weighted\ Averaged\ Precision = \Sigma\,(Precision_i * Support_i) / \Sigma\, Support_i$$

$$Weighted\ Averaged\ Recall = \Sigma\,(Recall_i * Support_i) / \Sigma\, Support_i$$

$$Weighted\ Averaged\ F1\ Score = \Sigma\,(F1\ Score_i * Support_i) / \Sigma\, Support_i$$

Model performance progression graph:

The BMWNet52 model's training process was monitored by analyzing the loss and accuracy graphs in Figure 6 throughout 20 epochs for both the training and validation sets.

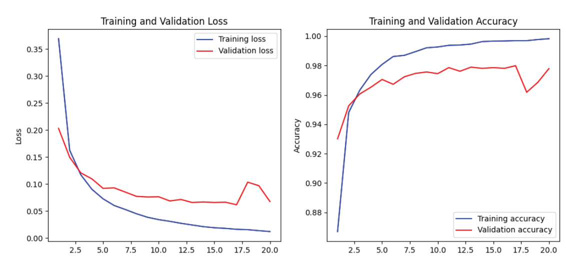

Figure 6: Training progression of the machine learning model over 20 epochs. The loss consistently decreased and accuracy consistently increased before starting to plateau at the 10th epoch, highlighting that further training beyond the 20th epoch would not improve performance.

The training loss curve consistently trended downwards, whereas the training accuracy trended upward. Both started to plateau at the 10th epoch. The validation metrics also followed the same trend but with more fluctuations. Initially, the validation accuracy was greater than the training accuracy

DOI: 10.36838/v6i10.11

but was overtaken by the 3rd epoch. The validation accuracy and loss began to plateau with minor upticks and downticks. Anomalously, at the 17th epoch, the validation loss increased significantly, and the validation accuracy decreased significantly, but it returned to the general trend at the 18th epoch. The plateauing of these metrics for both the training and validation sets indicated that further training beyond 20 epochs would not result in significant performance improvements.

Confusion Matrix:

A confusion matrix was used as a performance measurement tool to assess the classification model. It visualized the classifier's performance by tabulating the number of correct and incorrect predictions for each class. The confusion matrix comprehensively summarized the model's performance and helped identify misclassification patterns across different classes. In the confusion matrix shown in Figure 7, the true class labels are represented in the rows (Y-axis), whereas the predicted class labels are represented in the columns (X-axis).

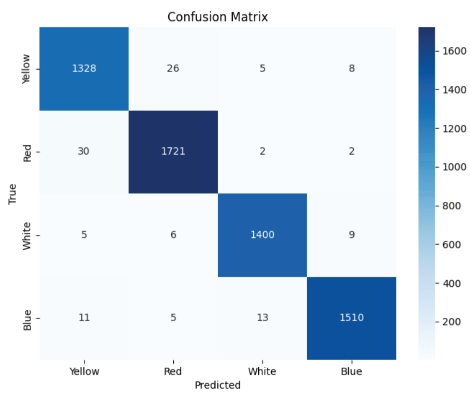

Figure 7: Confusion matrix comparing the number of predicted and true instances of each class in the validation set of the BMW-Seg-India dataset. Highlights the high true positive rate of the model with most images being accurately identified as belonging to the right class.

Each cell in the matrix represents the number of instances that belong to the true class (row) and were predicted as the corresponding predicted class (column).

True Positives (TP): The diagonal elements of the confusion matrix represent the number of instances correctly classified for each class. For example, in the cell (Y,Y), 1328 instances of the yellow class were correctly predicted to belong to the yellow class.

False Positives (FP): The off-diagonal values in each column of the confusion matrix represent the number of instances incorrectly classified as belonging to that class. For example, in the cell (Y,R), 26 images of the Yellow class were falsely predicted to belong to the Red class, a false positive for the yellow class.

False Negatives (FN): The off-diagonal values in each row of the confusion matrix represent the number of instances of that class that were incorrectly predicted as belonging to a different class. For example, in the cell (R,Y), 30 images that belonged to the red class were falsely predicted to belong to the yellow class, a false negative for the red class.

True Negatives (TN): The number of true negatives for a class is calculated by summing all instances that are neither in the row nor the column of the class in the confusion matrix, representing instances correctly predicted as not belonging to that class.

The confusion matrix revealed that the model performed well with the high counts along the diagonal, indicating that the model could accurately predict most instances for each class. Most misclassifications occurred between adjacent classes, with Y and R being confused with each other and W and B being confused with each other.

From the low misclassification rate shown in the confusion matrix in Figure 7 and the high Accuracy, Precision, Recall, and F1-score shown across all classes in Table 3, it is evident that the BMWNet52 Deep Learning Model with a Residual Network Architecture trained using Transfer Learning presents an effective solution for Automated BMW Segregation.

■ Conclusion

This study represents a novel effort in the domain of Automated BMW segregation by adhering to the guidelines outlined by the Government of India in the Biomedical Waste Management Rules, 2016. This research introduced the BMW-Seg-India dataset and the BMWNet52 model, highlighting the use of Residual Networks as an effective solution for segregating BMW according to these guidelines.

While this study focused on BMW segregation in India, the methodologies and findings can drive the use of transfer learning with the ResNet50 architecture for BMW classification tasks in other geographical regions, making the potential future impact global. This could improve BMW management practices, promoting safer and more efficient biomedical waste handling worldwide.

While this research contributes to the BMW management system, this field has greater potential. A significant opportunity lies in developing a fully Autonomous BMW Management System that seamlessly integrates segregation and disposal processes. This would improve efficiency and minimize workers' unnecessary exposure to hazardous waste.

■ Acknowledgments

Gratitude is extended to The Chairman of Kovai Medical Center and Hospital, Coimbatore, India, for granting the necessary permissions to photograph Biomedical Waste and the Infection Control Department for assistance in collecting and annotating the images.

■ References

1. World Health Organization. *Water, sanitation, hygiene, waste and electricity services in health care facilities: progress on the fundamentals.* www.who.int. https://www.who.int/publications/i/item/9789240075085.
2. World Health Organization. *Health-care waste*. WHO. https://www.who.int/news-room/fact-sheets/detail/health-care-waste.

3. Taslimi, M.; Batta, R.; Kwon, C. Medical Waste Collection Considering Transportation and Storage Risk. *Computers & Operations Research* **2020**, *120* (104966), 104966. https://doi.org/10.1016/j.cor.2020.104966.
4. Janik-Karpinska, E.; Brancaleoni, R.; Niemcewicz, M.; Wojtas, W.; Foco, M.; Podogrocki, M.; Bijak, M. Healthcare Waste—a Serious Problem for Global Health. *Healthcare* **2023**, *11* (2), 242. https://doi.org/10.3390/healthcare11020242.
5. Central Pollution Control Board. *Annual Report on Biomedical Waste Management as per Biomedical Waste Management Rules, 2016*; Central Pollution Control Board: Parivesh Bhawan, East Arjun Nagar, 2019. https://cpcb.nic.in/uploads/Projects/Bio-Medical-Waste/AR_BMWM_2019.pdf.
6. UNIDO; GEF; MoEFCC. *TRAINING MANUAL on BIO-MEDICAL WASTE MANAGEMENT for DOCTORS, NURSES, NODAL OFFICERS and WASTE MANAGERS*; Ministry of Environment and Forests, 2018. https://moef.gov.in/wp-content/uploads/2019/05/4.-doctorss-manual.pdf.
7. World Health Organization. *Safe management of wastes from health-care activities, 2nd ed*. www.who.int. https://www.who.int/publications/i/item/9789241548564.
8. Mitiku, G.; Admasie, A.; Birara, A.; Yalew, W. Biomedical Waste Management Practices and Associated Factors among Health Care Workers in the Era of the Covid-19 Pandemic at Metropolitan City Private Hospitals, Amhara Region, Ethiopia, 2020. *PLOS ONE* **2022**, *17* (4). https://doi.org/10.1371/journal.pone.0266037.
9. World Health Organization. *Safe Health-Care Waste Management WHO Core Principles for Achieving Safe and Sustainable Management of Health-Care Waste*; World Health Organization, 2007. https://noharm-global.org/sites/default/files/documents-files/2518/Safe_Healthcare_Waste_Mgmt.pdf.
10. Almuneef, M. Effective Medical Waste Management: It Can Be Done. *American Journal of Infection Control* **2003**, *31* (3), 188–192. https://doi.org/10.1067/mic.2003.43.
11. Datta, P.; Mohi, G.; Chander, J. Biomedical Waste Management in India: Critical Appraisal. *Journal of Laboratory Physicians* **2018**, *10* (1), 6. https://doi.org/10.4103/jlp.jlp_89_17.
12. Ministry of Environment, Forest and Climate Change. *Bio-medical_Waste_Management_Rules_2016*. dhr.gov.in. https://dhr.gov.in/sites/default/files/Bio-medical_Waste_Management_Rules_2016.pdf.
13. Singh, N.; Ogunseitan, O. A.; Tang, Y. Medical Waste: Current Challenges and Future Opportunities for Sustainable Management. *Critical Reviews in Environmental Science and Technology* **2021**, *52* (11), 1–23. https://doi.org/10.1080/10643389.2021.1885325.
14. Yu, Y. Deep Learning Approaches for Image Classification. In *Electronic Information Technology and Computer Engineering*; Association for Computing Machinery, 2023; pp. 1494–1498.
15. Alzubaidi, L.; Zhang, J.; Humaidi, A. J.; Al-Dujaili, A.; Duan, Y.; Al-Shamma, O.; Santamaría, J.; Fadhel, M. A.; Al-Amidie, M.; Farhan, L. Review of Deep Learning: Concepts, CNN Architectures, Challenges, Applications, Future Directions. *Journal of Big Data* **2021**, *8* (1). https://doi.org/10.1186/s40537-021-00444-8.
16. Sarkar, O.; Dey, A.; Malik, T. Modernized Management of Biomedical Waste Assisted with Artificial Intelligence. *International Journal of Biomedical and Clinical Analysis* **2023**, *3* (2), 69–86. https://doi.org/10.61797/ijbca.v3i2.265.
17. Zhou, H.; Yu, X.; Alhaskawi, A.; Dong, Y.; Wang, Z.; Jin, Q.; Hu, X.; Liu, Z.; Kota, V. G.; Abdulla, M. H. A. H.; Ezzi, S. H. A.; Qi, B.; Li, J.; Wang, B.; Fang, J.; Lu, H. A Deep Learning Approach for Medical Waste Classification. *Scientific Reports* **2022**, *12* (1). https://doi.org/10.1038/s41598-022-06146-2.
18. Bruno, A.; Martinelli, M.; Moroni, D. *Medical-Waste-4.0-Dataset: v1.0*. Zenodo. https://zenodo.org/records/7709001 (accessed 2024-05-27).
19. Pitakaso, R.; Khonjun, S.; Srichok, T.; Sethanan, K.; Nanthasamroeng, N.; Boonmee, C.; Gonwirat, S.; Luesak, P. *Pharmaceutical and Biomedical Waste*. www.kaggle.com. https://www.kaggle.com/datasets/engineeringubu/pharmaceutical-and-biomedical-waste (accessed 2024-05-27).
20. Kumsetty, N. V.; Nekkare, A. B.; S, S. K.; M, A. K. TrashBox: Trash Detection and Classification Using Quantum Transfer Learning. In *Open Innovations Association (FRUCT)*; IEEE, 2022.
21. Wangziang. *waste_pictures*. www.kaggle.com. https://www.kaggle.com/datasets/wangziang/waste-pictures.
22. Guo, X.; Yin, Y.; Dong, C.; Yang, G.; Zhou, G. On the Class Imbalance Problem. In *International Conference on Natural Computation*; IEEE, 2008.
23. Althnian, A.; AlSaeed, D.; Al-Baity, H.; Samha, A.; Dris, A. B.; Alzakari, N.; Abou Elwafa, A.; Kurdi, H. Impact of Dataset Size on Classification Performance: An Empirical Evaluation in the Medical Domain. *Applied Sciences* **2021**, *11* (2), 796. https://doi.org/10.3390/app11020796.
24. He, K.; Zhang, X.; Ren, S.; Sun, J. *Deep Residual Learning for Image Recognition*. arXiv.org [Preprint]. https://arxiv.org/abs/1512.03385.
25. Lin, K.; Zhao, Y.; Gao, X.; Zhang, M.; Zhao, C.; Peng, L.; Zhang, Q.; Zhou, T. Applying a Deep Residual Network Coupling with Transfer Learning for Recyclable Waste Sorting. *Environmental Science and Pollution Research* **2022**, *29* (60). https://doi.org/10.1007/s11356-022-22167-w.
26. Abood, I. N.; Al-Talib, G. A. A. Waste Classification Using Artificial Intelligence Techniques:Literature Review | Technium: Romanian Journal of Applied Sciences and Technology. *technium-science.com* **2023**, *5* (2023). https://doi.org/10.47577/technium.v5i.8345.
27. Basodi, S.; Ji, C.; Zhang, H.; Pan, Y. Gradient Amplification: An Efficient Way to Train Deep Neural Networks. *Big Data Mining and Analytics* **2020**, *3* (3), 196–207. https://doi.org/10.26599/bdma.2020.9020004.
28. Abd ElGhany, S.; Ramadan Ibraheem, M.; Alruwaili, M.; Elmogy, M. Diagnosis of Various Skin Cancer Lesions Based on Fine-Tuned ResNet50 Deep Network. *Computers, Materials & Continua* **2021**, *68* (1), 117–135. https://doi.org/10.32604/cmc.2021.016102.
29. Koonce, B. ResNet 50. In *Convolutional Neural Networks with Swift for TensorFlow*; Springer Link, 2021; pp. 63–72.
30. Huang, G.; He, J.; Xu, Z.; Huang, G. A Combination Model Based on Transfer Learning for Waste Classification. *Concurrency and Computation: Practice and Experience* **2020**, *32* (19). https://doi.org/10.1002/cpe.5751.
31. Zhao, Z.; Alzubaidi, L.; Zhang, J.; Duan, Y.; Gu, Y. A Comparison Review of Transfer Learning and Self-Supervised Learning: Definitions, Applications, Advantages and Limitations. *Expert Systems with Applications* **2024**, *242* (122807). https://doi.org/10.1016/j.eswa.2023.122807.
32. Deng, J.; Dong, W.; Socher, R.; Li, L.-J.; Li, K.; Fei-Fei, L. ImageNet: A Large-Scale Hierarchical Image Database. In *Computer Vision and Pattern Recognition*; IEEE, 2009.
33. Lin, M.; Chen, Q.; Yan, S. *Network in Network*; arXiv [Preprint], 2014. https://arxiv.org/pdf/1312.4400.
34. Garbin, C.; Zhu, X.; Marques, O. Dropout vs. Batch Normalization: An Empirical Study of Their Impact to Deep Learning. *Multimedia Tools and Applications* **2020**, *79* (19-20), 12777–12815. https://doi.org/10.1007/s11042-019-08453-9.

DOI: 10.36838/v6i10.11

35. Dwivedi, D.; Ganguly, A.; Haragopal, V. V. Contrast between Simple and Complex Classification Algorithms. In *Statistical Modeling in Machine Learning*; Elsevier, 2023.
36. Kingma, D. P.; Ba, J. *Adam: A Method for Stochastic Optimization*. arXiv.org. https://arxiv.org/abs/1412.6980.
37. Hassan, E.; Shams, M. Y.; Hikal, N. A.; Elmougy, S. The Effect of Choosing Optimizer Algorithms to Improve Computer Vision Tasks: A Comparative Study. *Multimedia Tools and Applications* **2022**, *82* (3), 16591–16633. https://doi.org/10.1007/s11042-022-13820-0.
38. N., C. B.; J., S. J. T.; Ruby, A. U.; Parveen, A. An Approach to Categorize Chest X-Ray Images Using Sparse Categorical Cross Entropy. *Indonesian Journal of Electrical Engineering and Computer Science* **2021**, *24* (3), 1700. https://doi.org/10.11591/ijeecs.v24.i3.pp1700-1710.
39. Mannor, S.; Peleg, D.; Rubinstein, R. The Cross Entropy Method for Classification. In *22nd International Conference on Machine Learning*; Association for Computing Machinery, 2005; pp. 561–569.

Authors

Srivatsav Kannan—I am in my junior year of high school and have a passion for all things related to technology. My primary research interest is exploring the intersection of machine learning and natural sciences. I am currently a research intern at the Coimbatore Institute of Technology.